RSC Advances

ROYAL SOCIETY OF CHEMISTRY

www.rsc.org/advances

Cite this: DOI:

www.rsc.org/xxxxxx

ARTICLE

Self-assembly of a hydrophobically end-capped charged amphiphilic triblock copolymer: Effects of temperature and salinity

Farinaz Kahnamouei[a], Kaizheng Zhu[a,], Reidar Lund[a], Kenneth D. Knudsen,[b] Bo Nyström[a*]

Received (in XXX, XXX) Xth XXXXXXXXX 2014, Accepted Xth XXXXXXXXX 20XX
DOI: 10.1039/b000000x

Abstract: The association properties of aqueous solutions of the anionic thermo-responsive triblock terpolymer *n*-octadecyl-poly(ethylene glycol)- *block*-poly(*N*-isopropyl acrylamide)-*block*-poly(2-acrylamido- 2-methyl-1-propanesulfonic sodium), abbreviated as C_{18}-PEG_{10}-*b*-$PNIPAAM_{54}$-*b*-$PAMPS_{10}$, have been studied as function of temperature and salinity. This polymer exhibits a lower critical solution temperature (LCST) owing to its PNIPAAM block, and the presence of charges at the end of the chain influences the interaction properties. The effect of ionic strength was examined in detail by means of turbidimetry, zeta-sizer, dynamic light scattering, densitometry, and small angle neutron scattering (SANS). A temperature increase was seen to promote the formation of large aggregates in this system, with a strong dependency on the ionic strength of the solution. Increasing the ionic strength was found to give a large and controllable decrease in the cloud point (CP) due to screening of the electrostatic interactions. The hydrodynamic radius was found to drop significantly upon addition of salt. At temperatures above CP, the intermicellar clusters observed by dynamic light scattering were found to contract. Furthermore, zeta-potential measurements demonstrated that charges were forced out towards the surface of the micellar structures with increasing temperature due to the strong dehydration effect of the associating PNIPAAM blocks.

Introduction

In the past few decades, there has been considerable interest in synthesis and characterization of amphiphilic block copolymers. Many of these have the ability to self-assemble into well-defined nano-structures in aqueous solutions.[1-5] Such copolymers may also contain a block or blocks that are able to undergo structural changes in response to external stimuli[6], giving them potential as constituents of new smart materials. In pursuit of this, materials that respond to different types of stimuli like temperature[7-9], ionic strength[10], pH[11,12], have been synthesized and are the subject of several studies. Many polymers exhibit a lower critical solution temperature (LCST), or upper critical solution temperature (UCST) behavior, promoting aggregation and macroscopic phase separation by increasing or lowering the temperature, respectively. A substantial amount of work has been carried out over decades to develop temperature sensitive polymers, of which some examples are given in references.[13-17] *N*-isopropylacrylamide (NIPAAM) is a temperature-responsive monomer that was first synthesized in the 1950s[18], and poly(*N*-isopropyl acrylamide), PNIPAAM, is the most universally studied thermo-responsive polymer in aqueous media.[19] High molecular weight PNIPAAM exhibits LCST behavior at around 32°C in water[19-21] and some degrees lower in physiological saline solutions. The LCST of PNIPAAM strongly depends on both the molecular weight and concentration of the polymer in the low molecular weight range.[22] By increasing the solution temperature towards the transition temperature, hydrophobic interactions will occur through isopropyl groups followed by creation of aggregates. In a recent study[23] it was argued that temperature dependent interactions between PNIPAAM and solutes arise because of changes in the local environment around the hydrophobic isopropyl domains. If the solution is not too dilute, macroscopic phase separation will eventually take place. The transition temperature is referred to as the LCST or the cloud point (CP).

By combining PNIPAAM with other polymeric blocks, one can modify the aggregation behavior of the polymer. One approach is to covalently connect a water-soluble block such as poly(ethylene glycol) (PEG) to a PNIPAAM block, resulting in a double hydrophilic PNIPAAM-*b*-PEG copolymer at low temperature. The resulting diblock polymer self-assembles into micelles with a dehydrated PNIPAAM core and dissolved PEG corona at temperatures above the transition temperature.[20] As an example, Motokawa et al[24] synthesized an amphiphilic block copolymer, PNIPAAM-*b*-PEG, with strong temperature-dependent solvent selectivity. The macroscopic observations (turbidity, fluidity and volume change) along with the microscopic observations (ultra-small and small-angle neutron scattering (USANS and SANS, respectively)) indicated various solution states. These states occur due to the interplay of short-range interactions among PNIPAAM, PEG block chains, and solvent, and long-range interactions arising from the elastic energy of PNIPAAM and PEG in the domain structures. Shi and coworkers[25] have studied the solution behavior of hydrophobically modified PNIPAAM. The copolymer of NIPAAM and octadecylacrylate (ODA) was synthesized and its aggregation and phase separation behaviors were investigated. It has been shown that even a minor amount of ODA can alter the amphiphilic properties of the polymer dramatically. Phase separation behavior was observed at 30°C,

which is lower than the corresponding transition of PNIPAAM itself.

In a recent work from our group[20], a non-ionic surfactant of PEG-octadecylether was grafted to PNIPAAM, and different end-capped *n*-octadecyl-PEG-*b*-PNIPAAM polymers were synthesized. At low temperatures, well-defined micellar structures were detected and by increasing the temperature up to near the LCST of PNIPAAM, the micelles were found to first collapse into smaller micelles, followed by inter-micellar aggregation and ultimately macroscopic phase separation. SANS and SAXS data analyses suggested a core-shell structure at moderate temperatures. At elevated temperatures, the formed micelles were found to shrink significantly, a behavior that was attributed to the collapse of PNIPAAM chains.

Micelles containing block polyelectrolytes, i.e., systems with a hydrophobic core and an ionic corona in aqueous media have also been studied. The primary work on these systems by Selb and Gallot was on micellization of polystyrene-*b*-poly(4-vinylpyridinium) copolymers in water-methanol-LiBr mixtures. It was demonstrated that the micelles have a star-like structure. The micellization process and micelle behavior were both found to be highly dependent on the solvent, temperature, salt concentration, and water-insoluble polystyrene block length.[26]

To date, several research groups have managed to synthesize and characterize[27,28] various thermo-responsive amphiphilic copolymers containing PNIPAAM, resulting in LCST behavior of the corresponding polymer solutions[21,22,29-31] and gels.[32,33] In the biomedical sciences, their ability to encapsulate hydrophobic drugs has attracted significant attention as possible drug delivery systems (DDS)[34,35], as have their potential for industrial applications.[36] The constant development of new drug delivery systems is driven by the necessity to maximize therapeutic activity, while minimizing undesirable side effects. In this context, drug delivery vehicles formed by self-assembly of amphiphilic block copolymers in aqueous solutions have received much attention during the past decades. One reason is that hydrophobic drugs can be encapsulated in the core of the micelles. Besides, the hydrophilic blocks, mostly composed of poly(ethylene oxide) (PEO) or PEG, are capable of establishing hydrogen bonds with the aqueous media and creating a firm shell around the micellar core.[2,13,37]

In the present study, we investigate the structures formed by a newly synthesized PNIPAAM-based block-copolymer, which has been supplied with an anionic group (PAMPS) and a hydrophobic end group (C_{18}). We follow in detail the interplay between charge, hydrophobicity and hydrophilicity on these structures, and show how temperature variations induce large changes in the system. The ionic strength is seen to be an important factor in the control of the behavior of this block copolymer. This work will elucidate the intricate interplay between hydrophobic interactions and electrostatic repulsive forces and the influence of the ionic strength on this balance. Understanding this competition between different interactions is important for gaining insight into the self-assembly process of amphiphilic entities and to be able to tailor-make systems for gene- and drug delivery applications.

Experimental

Materials

Poly(ethylene glycol) octadecyl ether (Brij®S10, M_n value of 711), 2-bromoisobutyl bromide and copper(II) chloride were all purchased from Sigma-Aldrich and employed as received. *N*-isopropylacrylamide (NIPAAM, Acros) was recrystallized from a toluene/*n*-hexane mixture and dried under vacuum prior to use. The charged monomer 2-acrylamido-2-methyl-1-propanesulfonic acid sodium salt, abbreviated as AMPS (50 wt% in H_2O, Aldrich), was purified from the trace inhibitor present in the sample by removing most of the water in the vacuum oven at 60°C, followed by washing with cold ethanol and finally drying under vacuum. Triethylamine (TEA) was dried over anhydrous magnesium sulfate, filtered, distilled under N_2 and stored over 4 Å molecular sieves. Copper (I) chloride from Aldrich was washed with glacial acetic acid, followed by washing with methanol and diethyl ether and then dried under vacuum and kept under N_2 atmosphere. *N*,*N*,*N'*,*N''*,*N'''*,*N''''*-(hexamethyl triethylene tetramine) (Me_6TREN) was synthesized according to a previous description in the literature.[38] All water used in this study was purified with a Millipore Mill-Q system and the resistivity was less than 18 M Ω cm.

Synthesis of the octadecyl-capped PEG initiator (C_{18}-PEG-Br)

The octadecyl-capped PEG macroinitiator (C_{18}-PEG-Br) was prepared by reacting poly(ethylene glycol) octadecyl ether (C_{18}-PEG-OH) with 2-bromoisobutyl bromide in the presence of triethylamine as outlined in Fig.1[20,39,40]. The ^{1}H-NMR spectrum indicated that the degree of esterification was at least 99 %.

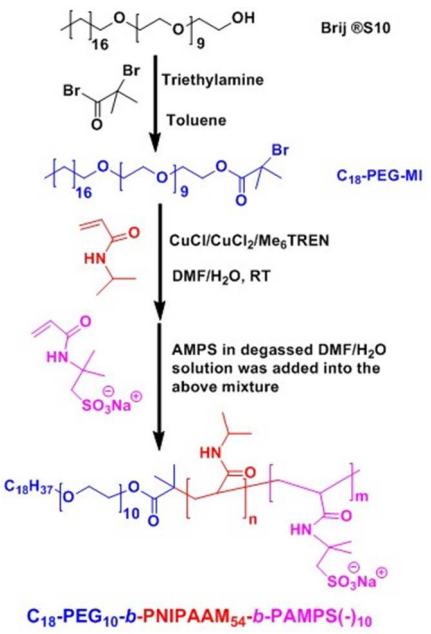

Fig 1 Synthetic route for the preparation of the triblock copolymer C_{18}-PEG_{10}-*b*-$PNIPAAM_{54}$-*b*-$PAMPS(-)_{10}$ *via* the 'one-pot' ATRP procedure.

The numbers of repeating units of the ethylene glycol (EG) in the PEG polymer was recalculated according to its proton NMR spectrum of the fully esterification product based on the corresponding integral area of the methenyl group of EG (-O-CH_2CH_2-) at 3.7 ppm and the integral area of the end-capped

methyl group (-C(CH_3)$_2$Br, 6H) at 1.8 ppm. The repeating units of EG are estimated to be 10 for Brij®S10, and it is denoted as C_{18}-PEG_{10}.[20,40]

Synthesis of the triblock copolymer

The triblock copolymer was prepared *via* a simple 'one-pot' two step ATRP procedure.[20,39-43] Briefly, the polymerization was performed in a water/DMF (40:60, v/v) mixture at 25 °C; the initiator/catalyst system in the mixture contained a PEG derivative macroinitiator (C_{18}-PEG_{10}-MI), CuCl, $CuCl_2$ and Me_6TREN (with molar feed ratio ([NIPAAM]=2M, [NIPAAM]/[AMPS]/[C_{18}-PEG_{10}MI]/[CuCl]/[$CuCl_2$]/[Me_6TREN] = 60/30/1/1/0.6/1.6). The preparation and purification procedure of the polymer was conducted under similar conditions as described in detail previously.[20,39-44]

The chemical structure and composition of the triblock copolymer was also ascertained by its ^{1}H NMR spectrum (Fig. 2). The number-average molecular weight and the unit numbers of *o*, *n* and *m*, in C_{18}-P(EG)$_o$-*b*-P(NIPAAM)$_n$-*b*-P(AMPS)$_m$ were evaluated by comparing the integral area of the methyne proton (number **8** in Fig. 2) of PNIPAAM (δ = 3.85 ppm, –C***H***(CH$_3$)$_2$, I_a), the methenyl proton of AMPS (number **13** in Fig. 2) (δ = 3.30 ppm, **–C*H*$_2$**SO$_3^-$, I_b), and the typical peak of the methenyl proton of EG (number **4** in Fig. 2) (δ = 3.70 ppm, -O**C*H*$_2$C*H*$_2$**O–, I_c) based on a simple equation: $m_{(NIPAAM)} = o \bullet 4(I_a/I_c)$; $n_{(AMPS)} = o \bullet (2I_b/I_c)$. The composition of the triblock copolymer is estimated to be: *o*/*m*/*n* = 10/54/10, i.e., C_{18}-PEG_{10}-*b*-P(NIPAAM)$_{54}$-*b*-P(AMPS(-))$_{10}$, based on our previous calculation results that the numbers of repeating units of the ethylene glycol of C_{18}-PEG-MI is 10.[20,40]

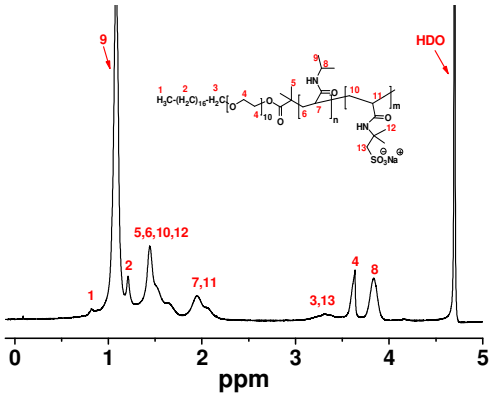

Fig 2 ^{1}H NMR spectrum of octadecyl-capped triblock copolymer C_{18}-PEG_{10}-*b*-PNIPAAM$_{54}$-*b*-PAMPS$_{10}$(-) (D_2O as solvent, 300 MHz).

Asymmetric flow field-flow fractionation

The asymmetric flow field-flow fractionation (AFFFF) measurements were carried out on an AF2000 FOCUS system (Postnova Analytics) equipped with an RI detector (PN3140) and a multiangle (7 detectors in the range 35 to 145°) light scattering detector (PN3070, λ = 635 nm). The sample (0.5 wt % in 0.1 M NaCl) was measured at 5 °C (to suppress the formation of aggregates) using a 350 μm spacer, a regenerated cellulose membrane with a cut-off of 5000 (Z-MEM-AQU-426N, Postnova), and an injection volume of 20 μL. In the experiments a constant detector flow rate of 0.3 mL/min and a slot pump flow rate of 1.5 mL/min were used. The focusing time was 10 min at a cross-flow of 2.0 mL/min. The cross-flow was then linearly reduced to zero during a period of time of 7 min. Processing of the measured data was achieved by the Postnova software (AF2000 Control, version 1.1.011). The molecular weight and polydispersity of the sample (Fig. 3) was determined using this software with a Zimm-type fit. The molecular weight measured by AFFFF ($2.8x10^4$ g/mol) is higher than the structure determined by NMR would suggest ($9.2x10^3$ g/mol). The reason for this may be that even though the AFFFF experiments were conducted at a low temperature and a low polymer concentration, some small aggregates may form and affect the molecular weight determination.

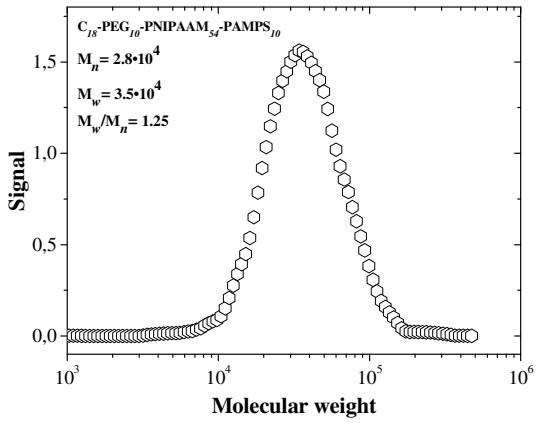

Fig 3 The molecular weight distribution curve of C_{18}-PEG_{10}-*b*-PNIPAAM$_{54}$-*b*-PAMPS(-)$_{10}$ in dilute aqueous solution (0.1 M NaCl) at 5 °C by means of AFFFF.

Zeta-potential experiments

Zeta-potential measurements were made with a Zeta-sizer Nano ZS instrument, Malvern instruments, Ltd. The sample cell was a "dip" cell with palladium electrodes with 2 mm spacing, a PCS1115 cuvette, and a cap. The instrument determines the electrophoretic mobility of the sample by means of Laser Doppler Velocimetry (LDV) and the zeta potential is calculated from these measurements on the basis of the Henry equation that relates the zeta potential, ζ, to the electrophoretic mobility, U_E (Eq.(1))

$$U_E = \frac{2\varepsilon\zeta}{3\eta} f(Ka) \quad (1)$$

where η and ε are the solvent viscosity and the dielectric constant, respectively, at a given temperature. The Smoluchowski approximation to Henry's function ($f(Ka)$=1.5) was applied.[45,46]

The experiments were carried out at several temperatures with small intervals around the cloud point. The equilibrium time at each temperature was 150 seconds. The zeta potential values presented in this study are the averages calculated on the basis of three runs both for a -68 mV standard and the samples.

Turbidimetry

The dependence on temperature of the transmittance and cloud point of the solutions was determined via a NK60-CPA cloud point analyzer from Phase Technology. Phase changes of the sample are here registered by a scanning diffusive light scattering technique with high sensitivity. A light beam from the employed AlGaAs light source (654 nm), with a typical spectral half-width of 18 nm, is focused on the measuring sample. Directly above the sample is an optical system that monitors the scattered intensity signal (S) of the sample while it is subjected to prescribed temperature alterations.[22,47,48] The relation between the calculated turbidity (τ) from the spectrophotometer experiments and the signal (S) from the cloud point analyzer is given by Eq.(2).[48]

$$\tau(cm^{-1}) = 9.0 \times 10^{-9} S^{3.751} \quad (2)$$

For the measurements, 0.15 mL of the test solution is applied by a micropipette onto a specially designed glass plate. The plate is coated with a thin metallic layer functioning as a high reflectivity mirror. The sample surface is covered with highly transparent silicon oil in order to avoid evaporation of solvent at higher temperatures. A platinum resistance thermometer probes the temperature of the sample, and a compact thermoelectric device (array of Peltier elements) located close to the test solution is utilized to cool down and warm up the sample over a wide range of temperatures (–60 to +60°C). In this work, the heating rate was set to 0.2°C/min, and no effect of the heating rate on the signal was observed at low heating rates. All data from the cloud point analyzer will in this work be reported in terms of turbidity (Eq. (2)).

Dynamic Light scattering (DLS)

DLS experiments were conducted with the aid of a multi-angle light scattering (MALS) spectrometer with vertically polarized incident light, which is supplied by a helium-ion laser with λ=632.5 nm. The beam is focused onto the sample cell through a temperature-controlled chamber.

In the light scattering experiments we probe a wave vector $q = \left(\frac{4\pi n}{\lambda}\right)\sin(\frac{\theta}{2})$, where λ is the wavelength of the incident light in a vacuum, θ is the scattering angle and n is the refractive index of the medium. If the scattered field obeys Gaussian statistics (as for the present samples) the measured correlation function $g^2(q,t)$ can be related to the theoretically amenable first-order electric field correlation function $g^1(q,t)$ by the Siegert relationship $g^2(q,t) = 1 + B\,|g^1(q,t)|^2$, where B is an instrumental parameter.

For dilute solutions of associating copolymers containing complexes with different sizes, the non-exponential behavior of the autocorrelation function can be portrayed by using a Kohlrausch-Williams-Watts[49,50] stretched exponential function. This approach is found to well describe the correlation function data in this work, and the algorithm employed in the analysis of the present correlation function data can be cast in the following form

$$g^1(t) = \exp[-(t/\tau_{fe})^{\beta}] \quad (3)$$

The correlation functions were analyzed by using a nonlinear fitting algorithm (a modified Levenberg-Marquardt method) to attain best-fit values of the parameters τ_{fe} and β appearing on the right-hand side of Eq 3. A fit was considered to be satisfactory if there was no systematic deviation in the plot of the residuals of the fitted curve and the values of the residuals were small. The mean relaxation time is given by Eq. (4):

$$\tau_f = \frac{\tau_{fe}}{\beta}\Gamma(\frac{1}{\beta}) \quad (4)$$

where the variable τ_{fe} is an effective relaxation time, and β ($0 < \beta < 1$) is a measure of the width of the distribution of relaxation times. The width of the distribution decreases as the stretched exponent approaches 1. $\Gamma(\frac{1}{\beta})$ is the gamma function of $\frac{1}{\beta}$. For the time correlation function of the concentration fluctuations in the domain $qR_h < 1$ (R_h is the hydrodynamic radius), the time behavior is related to the mutual diffusion coefficient, D, *via* $\tau_f^{-1} = Dq^2$. When the mode is diffusive and we consider dilute solutions, the apparent hydrodynamic radius R_h (assuming that we have spherical entities) is related to D via the Stokes-Einstein relationship, $D = \frac{k_B T}{6\pi\eta_0 R_h}$, where k_B is the Boltzmann constant and η_0 is the viscosity of the solvent at the absolute temperature T.

Densitometry

The lower critical solution temperature (LCST) of the polymer solutions may also be studied via densitometry. Solution density measurements were performed on a DMA5000 densitometer (Anton Paar). The densities are determined by an oscillating tube technique that exploits the relationship between the period of oscillation and fluid density.[31,51,52] The tube containing fluid is oscillated at resonant frequency by electromagnetic vibrators. The resonant frequency can thus be measured with high accuracy. The tube is isolated from the fixtures by carefully designed bellows.[53] The apparent partial specific volume, v_{solute}, of the solute is determined from density measurements of a solution with solute and of pure solvent as shown in Eq. (5):

$$v_{solute} = \left(\frac{1}{c_{solute}}\right)\left(\frac{1}{d_{solute}}\right) - \left(\frac{1 - c_{solute}}{c_{solute}}\right)\left(\frac{1}{d_{solvent}}\right) \quad (5)$$

where c_{solute} is the weight fraction of the solute, and d_{solute} and $d_{solvent}$ are the measured densities of the solution with the solute and of the pure solvent, respectively.[31,51,52] The relation holds when the viscosity of the sample is relatively low, as it is for the samples in the present work.

The sample volume needed for density measurements is approximately 1.5 ml. Densities were measured for 0.5wt% polymer solutions in water as well as in the presence of 0.05M, 0.1M, 0.5M, and 1M NaCl solutions in steps of 1 degree from 5 to 50 °C. The densitometer was calibrated at 20 °C, using air and Millipore water as reference samples. In the temperature range from 20 °C to 50 °C the accuracy of the measurement is 0.000020 g/cm^3, and it is 0.000050 g/cm^3 from 55 to 90 °C. Because of the relatively low concentration of polymer, the derived apparent partial specific volumes have an accuracy of about 0.1-0.3%.[51]

Small Angle Neutron Scattering (SANS)

The SANS-instrument at the JEEP-II reactor of IFE at Kjeller, Norway, was employed for the small angle neutron scattering measurements. The wavelength was set with the aid of a velocity selector (Dornier), using a wavelength resolution ($\Delta\lambda/\lambda$) of 10%. The neutron detector was a 128x128 pixel, ^{3}He -filled RISØ type, mounted on rails inside an evacuated detector chamber. The investigated scattering vector q-range was $8\times10^{-3} \leq q \leq 0.3$ Å^{-1}. In all the SANS measurements, deuterium oxide (D_2O) was used as a solvent instead of H_2O in order to obtain good contrast and low background for the neutron-scattering experiments. The samples were introduced into 5 mm quartz cuvettes. To ensure good thermal contact, the measuring cells were placed onto a copper-base and mounted onto the temperature-controlled sample stage. The detector chamber was evacuated to reduce the scattering caused from air. Standard reductions of the scattering data, including transmission corrections, were done by including data collected from empty cell, beam without cell, and blocked-beam background. The data were converted to an absolute scale (coherent differential cross section ($d\Sigma/d\Omega$)) via normalization based on direct beam measurements.

For the situations where individual micelles were formed, a model fitting of the scattering data was made (on an absolute scale) taking into account the molecular parameters of the system. The scattering length densities (ρ) for neutrons were calculated based on the densities reported in literature for PEG and C_{18}.[48] Based on these values we obtain for C_{18} that $\rho = -0.34\cdot10^{10}$ cm^{-2}, and for PEG $\rho = 0.64\cdot10^{10}$ cm^{-2}. For PAMPS, using a density of 1.25 g/mL at 20 °C, a value of ρ equal to $7.3\cdot10^{9}$ cm^{-2} is obtained. Finally, for PNIPAAM the density was measured to be 1.136 g/mL at 20 °C, leading to $\rho = 0.84\cdot10^{10}$ cm^{-2}.

In the data modelling we assumed that micelles can be described by a core-shell form factor. The core-shell model can be written on the following form assuming monodisperse star-like micellar entities.[20,54,55]

$$
\begin{aligned}
I(Q) = \frac{\varphi}{PV_{BCP}} [&\Delta\rho_{cp}^2 P^2 V_{cp}^2 A(Q)_c^2 \\
&+ \Delta\rho_{sp}^2 P (P - F(0)_{blob}) V_{sp}^2 A(Q)_{sh}^2 \\
&+ 2\Delta\rho_{cp}\Delta\rho_{sp} P^2 V_{PEO} V_{cp} A(Q)_c A(Q)_{sh} \\
&+ V_{sp}^2 \Delta\rho_{sp}^2 F(Q)_{blob}]
\end{aligned}
\tag{6}
$$

where P is the aggregation number (average number of chain per micelle), φ is the volume fraction, $V_{BCP} = V_{cp} + V_{sp}$ is the total molar volume of the block copolymer. V_{cp} is the volume of the core constituent (here mainly C_{18}) and V_{sp} is given by: $V_{sp} = V_{PNIPAAM}+V_{PEG}+V_{PAMPS}$. $\Delta\rho_i = \rho_i-\rho_0$ is the contrast determined by the scattering length density difference between the polymer block (shell-forming polymer ($i=sp$) or core-forming polymer ($i=cp$)) and the solvent ($i=0$). F(Q) is the form factor of a single polymer chain. The scattering amplitude of the shell, $A(Q)_{sh}$ was calculated using:

$$
A(Q)_{\mathrm{sh}} = \exp\left(-Q^2\sigma_{\mathrm{int}}{}^2/2\right)\frac{1}{C}\int_{\mathrm{Rc}}^{\infty} 4\pi r^2 n(r)\frac{\sin(Qr)}{Qr}\mathrm{d}r \tag{7}
$$

Here σ_{int} is the width of the core-corona interface and R_c is the radius of the core. n(r) is a density profile for the corona for which we chose a flexible power-law profile multiplied with a cut-off function:

$$
n(r) = \frac{r^{-x}}{1 + \exp\left((r - R_{\mathrm{m}})/\sigma_{\mathrm{m}}R_{\mathrm{m}}\right)} \tag{8}
$$

where R_m and σ_m are the outer cut-off radius and smearing of the density profile, respectively, and x is a scaling exponent that takes a value of x=4/3 for star-like structures.[56-58] For the micellar core the scattering amplitude is:

$$
A(Q)_{\mathrm{c}} = \exp\left(-Q^2\sigma_{\mathrm{int}}{}^2/2\right)\frac{3\left(\sin(QR_{\mathrm{c}}) - QR_{\mathrm{c}}\cos(QR_{\mathrm{c}})\right)}{(QR_{\mathrm{c}})^3} \tag{9}
$$

In addition a constant, B, was added to take into account a Q-independent background in the SANS data.

Results and discussion

3.1. Turbidimetry

A distinct feature of a thermo-responsive block copolymer is that by going above a certain temperature, the turbidity of the polymer solution undergoes major changes. The block copolymer studied here, demonstrated such LCST behavior, which means that the solutions tend to phase separate at elevated temperatures due to a continuous growth of the hydrophobic microdomains.

Quan et al[20] have performed turbidity measurements on PNIPAAM homopolymer, as well as on C_{18}-PNIPAAM and C_{18}-PEG-PNIPAAM. They showed that PNIPAAM exhibits a sharp transition to a turbid solution at the approximate temperature of

34-35 °C. For the end-capped C_{18}-PNIPAAM, a certain value of turbidity was detectable even at low temperatures, and the cloud point was observed to shift downwards to 32 °C. For the C_{18}-PEG-PNIPAAM copolymers with long PEG spacers, the cloud point was shifted to higher temperature, about 40 °C, due to the increased solubility of PEG and formation of more stable micelles

The block copolymer in the present study has been investigated both in water and saline solutions as a function of temperature. Generally, increase in the turbidity with increasing temperature reveals the formation of inter-micellar structures. When the PNIPAAM block is sufficiently long, the PNIPAAM segments contract to avoid water exposure.[39] When the ionic strength is increased in the polymer solution by adding salt, the surface charges of the micelles will be screened. The repulsive forces, which hindered aggregation are thus weakened or removed (depending on the ionic strength), and aggregation of micelles occur at lower temperatures.

The temperature dependencies of the turbidity for 0.5 wt% polymer solutions in the absence of salt and with different salt concentrations are illustrated in Fig. 4. It can be seen (Fig. 4a) that the transition in turbidity is shifted towards lower temperatures as the salt concentration increases, as expected. The inset shows how the CP changes with salt concentration. By increasing the temperature well above CP, macroscopic phase separation occurs and as a result the turbidity remains almost constant above a certain temperature (when measured via a reflective mirror system as done here).

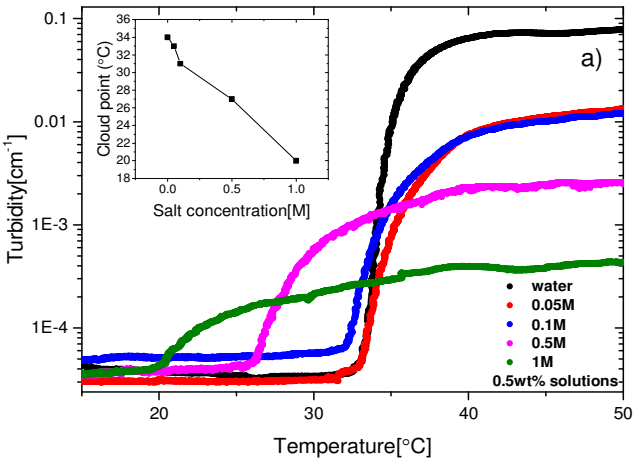

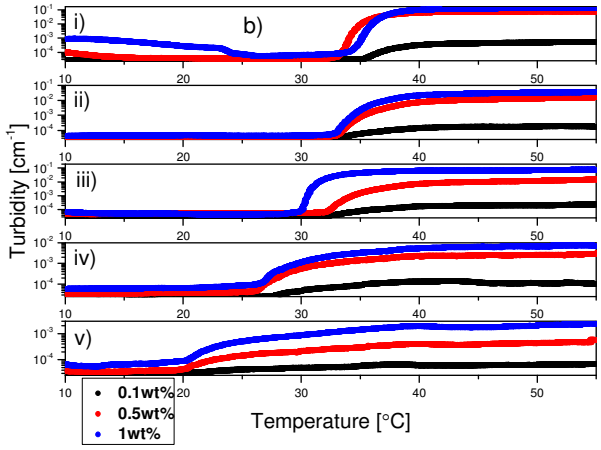

Fig 4. a) Turbidity versus temperature for 0.5 wt% solutions of C_{18}-PEG_{10}-*b*-$PNIPAAM_{54}$-*b*-$PAMPS_{10}$ at different salt concentrations. The inset shows the effect of salt addition on the cloud point. b) Turbidity versus temperature for 0.1wt%, 0.5wt% and 1wt% solutions of C_{18}-PEG_{10}-*b*-$PNIPAAM_{54}$-*b*-$PAMPS_{10}$ in i) water, ii) 0.05M NaCl, iii) 0.1M NaCl, iv) 0.5M NaCl, and v) 1M NaCl.

Fig. 4b shows the effect of change in polymer concentration on the behavior of the turbidity at different salt concentrations. We see that there is a general trend of a slight lowering in CP when the polymer concentration is increased from 0.1 to 1.0wt%, a result that is reasonable since an increased concentration will raise the probability of hydrophobic segments interacting at a given temperature.

Zeta-potential measurements

Zeta-potential experiments were performed to obtain information on the colloidal stability of the micellar structures formed. In general, the colloidal stability depends on the balance of Van der Waals attractions, hydrophobic interactions, electrostatic repulsion, and steric forces.[61] The surface charge of the polymeric micelles was determined over a wide temperature interval. The measurements were carried out on dilute (0.1 wt%) salt-free solutions of the block copolymer. The polymer solution remained homogeneous and no sign of sedimentation was observed through the whole temperature range for this concentration. The inset in Fig 5 shows that both elevated temperature and high salinity promote enhanced turbidity. The zeta-potential measurements of the micellar structures from 25 to 45°C disclose temperature-induced response as well as micellar stability (Fig. 5). The negative zeta-potential values are the result of the -SO_3^- functional groups of the charged PAMPS block. By raising the temperature, the absolute values of the negative zeta-potentials are found to increase. It is known[16,,60] that at elevated temperature, charges can be forced out towards the surface of micelles and inter-micellar aggregates, due to the hydrophobic contraction of the micelle. The observed trend of increasing absolute values of the zeta potential is compatible with the overall decreased micellar sizes seen from DLS measurements, as will be demonstrated later (Fig 9). The rate of this increase becomes stronger as the cloud point of the solution is passed, which is at ca. 34°C for the salt-free solution (cf. Fig 4). This can for our

system be attributed to the collapse of the PNIPAAM block[61] at elevated temperatures. When reaching the LCST, the hydrophobic interaction between the PNIPAAM blocks induces contraction and an outward movement of the charged groups. A similar behavior has been observed for positively charged PNIPAAM-containing diblock copolymers.[16,60]

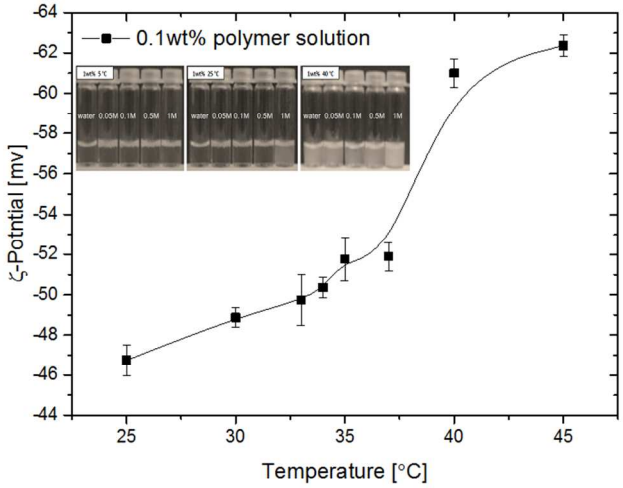

Fig 5 Zeta potential versus temperature for 0.1 wt% solution of the block copolymer in water. Inset: Visual appearance of 1wt% solutions of C_{18}-PEG_{10}-*b*-$PNIPAAM_{54}$-*b*-$PAMPS_{10}$ in water, 0.05M NaCl, 0.1M NaCl, 0.5M NaCl, and 1M NaCl at the temperatures of 15°C , 25°C, and 40°C.

Dynamic light scattering

Dynamic light scattering (DLS) was employed to investigate the hydrodynamic radii and dynamics of the micelles, and their temperature and ionic strength dependencies. The normalized homodyne intensity autocorrelation function $g^2(t)$ was measured simultaneously at 8 angles starting at θ=22° with 17° intervals. Eq. 3 was employed in the analysis of the DLS data.

To compensate for simple temperature-induced changes in solvent viscosity, the first-order electric field autocorrelation function, $g^{(1)}(t)$, was plotted against tT/η_0 (where t is the time, T is the absolute solution temperature, and η_0 is the solvent viscosity). This is shown in Fig 6a for the 0.5wt% solution at various temperatures in salt-free solution.

Fig 6 a) First-order electric field autocorrelation function versus tT/η_0 for 0.5 wt% solution of C_{18}-PEG_{10}-*b*-$PNIPAAM_{54}$-*b*-$PAMPS_{10}$ in salt-free solution at a scattering angle of 107°. b) Plot of $g^{(1)}$ (t) versus time at different scattering angles and their corresponding fits of 0.5wt% solution of the copolymer. The inset shows a plot of $g^{(1)}$ (t) versus q^2t, demonstrating the diffusive behavior of the system. c) The decay of a correlation function (at a scattering angle of 107° and a temperature of 25°C), together with a fit of Eq. (3), for a polymer concentration of 0.5 wt%. The inset shows a plot of the corresponding residuals which are small and non-systematic.

As a general trend, the decay of the autocorrelation function is expected to be shifted to shorter times for smaller particles. A close inspection of the correlation functions in Fig. 6a reveals that a shorter relaxation time starts to appear at a temperature of ca. 35°C. This is due to hydrophobically-induced compaction of the micelles. Fig. 6b shows the correlation functions at various scattering angles and their corresponding fits for 0.5wt% C_{18}-PEG_{10}-*b*-$PNIPAAm_{54}$-*b*-$PAMPS_{10}$ in water at 25 °C. The inset plot in Fig. 6b, where the inverse relaxation time is plotted versus q^2 for different scattering angles, illustrates that the relaxation process is diffusive (q^2-dependent).

To demonstrate the typical goodness of the fitting procedure, and to endorse the functional form of the fitting algorithm that is used to portray the correlation functions, the decay of the correlation function at an angle of 107°, together with a stretched exponential fit, is plotted in Fig. 6c. The inset plot shows the random distribution and small values of the residuals, demonstrating a good agreement between the correlation function and the fit.

The copolymer studied here is both charged and temperature-sensitive and below we discuss how temperature and salt addition affect the size of the species. From the Stoke-Einstein relationship, the values of the apparent hydrodynamic radii can be calculated, and the values of R_h as function of temperature for a 0.5 wt% copolymer solution in the presence of different levels of salt addition are displayed in Figure 7.

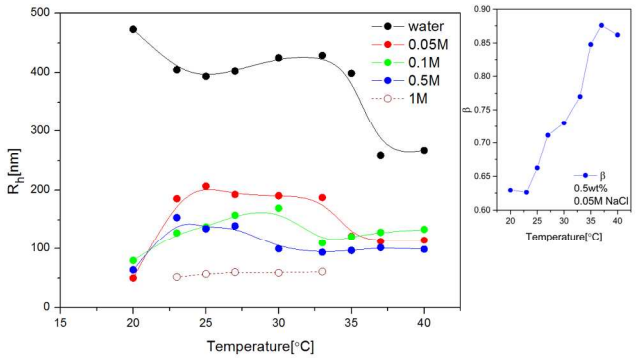

Fig 7 Hydrodynamic radii versus.temperature for 0.5 wt% samples at different ionic strengths. To the right the stretched exponent β versus temperature is shown for the sample with 0.05 M NaCl.

Let us first discuss the behavior for the solution without added salt. In this case, R_h decreases initially and at intermediate temperatures a plateau-like region is formed. Subsequently, at temperatures above CP, R_h falls off. This behavior can be rationalized in the following way. Since the species are in the range around 400 nm, this suggests that even at ambient temperature intermicellar structures are formed at this concentration. The initial decrease of R_h indicates a temperature-induced compaction of these complexes. At intermediate temperatures, a modest change of R_h takes place and this may be attributed to the competition between electrostatic expansion and hydrophobic contraction. Although the hydrophobic association effect is enhanced at elevated temperatures, this effect is counteracted by the augmented electrostatic repulsive forces (cf. Fig. 5) at higher temperatures. At temperatures above CP, the hydrophobic contraction effect prevails and R_h drops. Addition of salt significantly reduces the size of the complexes. At 20 °C in the presence of salt, the level of salt addition has very little influence on the size (Fig 7). The reason for the drastic drop of R_h is ascribed to screening of electrostatic repulsive forces. The general trend at all salt concentrations, except the highest, is that the clusters grow at intermediate temperatures. Above CP, the species shrink due to the dominance of the hydrophobic compression of the species. At the highest salt concentration, we do not observe any influence of temperature on R_h in the considered temperature domain. At this high level of salt addition, the polymer solution becomes highly turbid at elevated temperatures and severe multiple scattering prevents proper analysis of the correlation functions. Thus, the values indicated for R_h in the case of 1M NaCl are influenced by this. At high ionic strength of the polymer solutions, the presence of the Cl^- anion, due to its location in the Hofmeister series[62], frequently leads to higher surface tension, lower solubility of the macromolecules, and salting-out effects (aggregation of molecules).[62,64] At high salinity, we may in a narrow temperature interval have a situation where the growth and contraction effect counteract each other so the size of the complexes is virtually constant. The inset plot (results for a 0.5 wt% copolymer solution in the presence of 0.05 M NaCl) shows that the value of β rises strongly as the temperature increases. This trend is similar for the other levels of salt addition. The distribution of relaxation times thus becomes narrower at higher temperatures, and β approaches its ultimate value of 1, suggesting that the complexes formed at elevated temperatures are of nearly the same size. This type of cluster growth behavior has been reported and discussed[16] previously for a charged diblock copolymer.

Densitometry

The apparent specific volume of C_{18}-*b*-PEG_{10}-b-$PNIPAAm_{54}$-*b*-$PAMPS_{10}$ as a function of temperature was determined *via* Eq. (5) from density measurements in a temperature range of 5 to 50 °C (Fig 8). For all the samples an increase in the specific volume was detected with increasing temperature. This trend has also been observed for the octadecyl chain alone in the micellar state, and for PEO both in the micellar state and in the form of homopolymer[52], being consistent with the increase in thermal motion. The sample with the highest ionic strength has the lowest specific volume, i.e., the highest specific density, in accordance with the observed size reduction due to the salt screening effect commented on in the previous section (Fig. 7). The observed transition temperature for the specific volume correlates well with the value of the cloud points based on turbidity measurements (see inset Fig 4). The shift of the transition point to lower temperatures with increasing level of salt addition is probably related to a collapse of the PNIPAAM block as discussed previously.[65,66]

A mapping of the specific volume of each block is helpful for the interpretation of the behavior of the polymer, and can be used as input for subsequent SANS modelling. The data can be found in Table S1 (supplementary information). For the PNIPAAM homopolymer, the density was measured by densitometry and the specific volume was calculated from Eq. (5). For C_{18} and PEG the specific volumes have been taken from the work of Sommer and Pedersen.[52] Approximate specific volume of PAMPS could then be calculated based on our density measurements for the whole C_{18}-PEG_{10}-*b*-$PNIPAAM_{54}$-*b*-$PAMPS_{10}$ polymer.

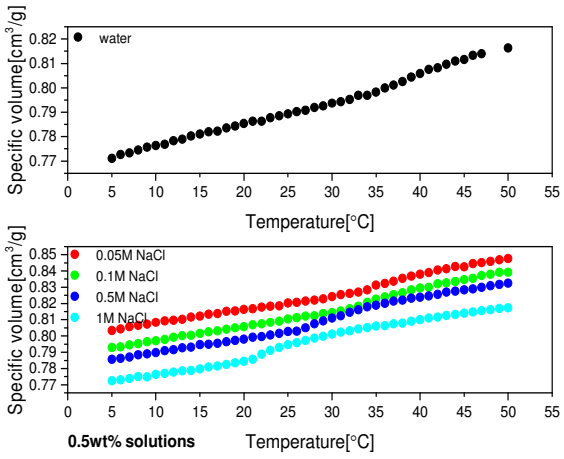

Fig 8 Specific volume of 0.5 wt% C_{18}-PEG_{10}-*b*-$PNIPAAM_{54}$-*b*-$PAMPS_{10}$ in water, and at different levels of salt addition in a temperature range of 5 to 50 °C.

SANS-measurements

Fig. 9 shows SANS patterns versus temperature for 0.5 wt% solutions of the copolymer with increasing amounts of added salt (data for other ionic strengths, 0.05 and 0.5 M, as well as SANS data without polymer present, can be found in Fig.S1-S2 in the supplementary information). Already by visual inspection we can see that a strongly increased scattering, related to size increase in the nano-range, commences above a certain temperature. The effect is seen most clearly for the high ionic strength (1M NaCl). The threshold temperature is also seen to become lower as the salt concentration is increased. For comparison, scattering data for the solution without polymer is also shown (1M NaCl/D_2O). As expected, the contribution from the solvent, even with 1M NaCl, is much lower (about a factor of 100) than that of the polymer solution.

We see that for the highest salt concentration the increased scattering has started already at 20 °C, which is reasonable since CP was measured to 20 °C for this system (see Fig. 4a). For the sample without salt the changes are more moderate, but there are some systematic changes (increased low-q scattering) with increasing temperature. This corresponds well to the evolution of the specific volume for this sample (Fig. 8). The major changes for this sample are not seen until above 35 °C, which is the CP of the pure polymer in D_2O. For other ionic strengths, there is a continuous trend of change between these two temperature extremes (cf. also Supporting Information). The SANS data therefore seem to correlate well with the results described earlier from both turbidity and specific volume measurements.

Below the cloud point temperature, we see a flattening of the scattering curves at low q (plateau-like) for all samples. This is indicative of separate entities with sizes well within the nano-range. For the 1M NaCl sample, for example, the plateau region that we see starting between 0.01 and 0.02 $Å^{-1}$ at 15 °C, is indicative of such structures.

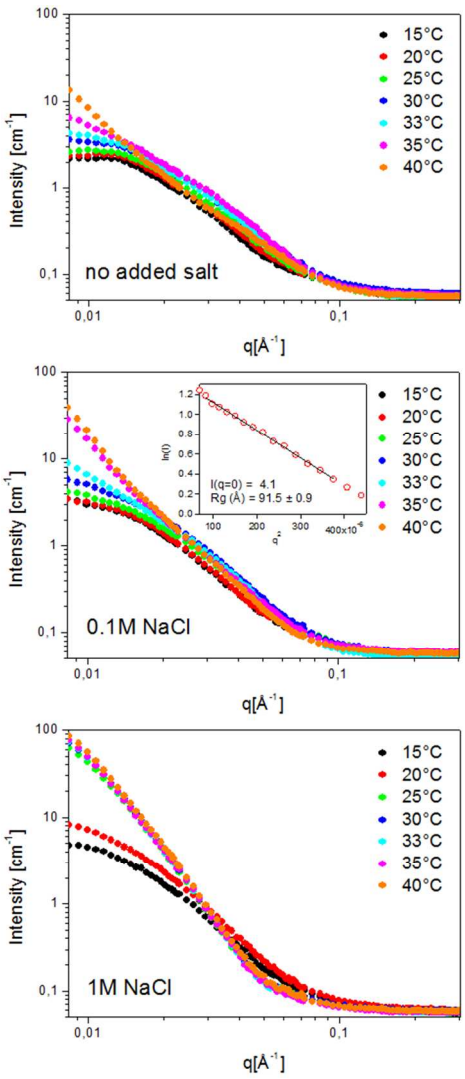

Fig 9 SANS patterns of 0.5wt% C_{18}-PEG_{10}-*b*-$PNIPAAM_{54}$-*b*-$PAMPS_{10}$ solutions at different salinity in a temperature range of 15 to 40 °C. Inset: Guinier fit for the polymer solution in the presence of 0.1 M NaCl at 15°C.

A simple Guinier plot of this data, shown in the inset, gives an R_g-value just below 100 Å (10 nm). This is in relatively good agreement with the DLS data for this sample, taking into account that DLS measures also the hydration layer connected with the micelle.

At temperatures above the cloud point, all samples show strongly increased scattering at low q, demonstrating the existence of large aggregates. These are larger than what can be directly determined by SANS, since there is no sign of a low-q plateau. This is in

accordance with the turbidity data (Fig. 4) that indicated large structures at these temperatures, as well as with DLS data (Fig. 9) that shows structures well above 100 nm at these temperatures.

The behavior with varying ionic strength can alternatively be illustrated by selecting one temperature and inspecting how the different samples - with CPs below and above that temperature - behave. For the plots in Fig. 10, temperatures of 15, 30, and 40 °C have been chosen. We now see clearly how the samples with the highest ionic strengths, and with CPs below 30 °C (27 and 20 °C for 0.5 and 1M NaCl, respectively), exhibit a 10-fold stronger scattering compared with the others indicating larger aggregates (Fig 10b). As expected, the samples with low ionic strengths, having CPs well above 30°C, show scattering typical of smaller entities, as mentioned before. For the sample in 0.1 M NaCl, the CP was measured to 31°C (Fig 4), thus the data in Fig 10b correspond to just the edge of the transition, without being manifested on the nanoscale yet.

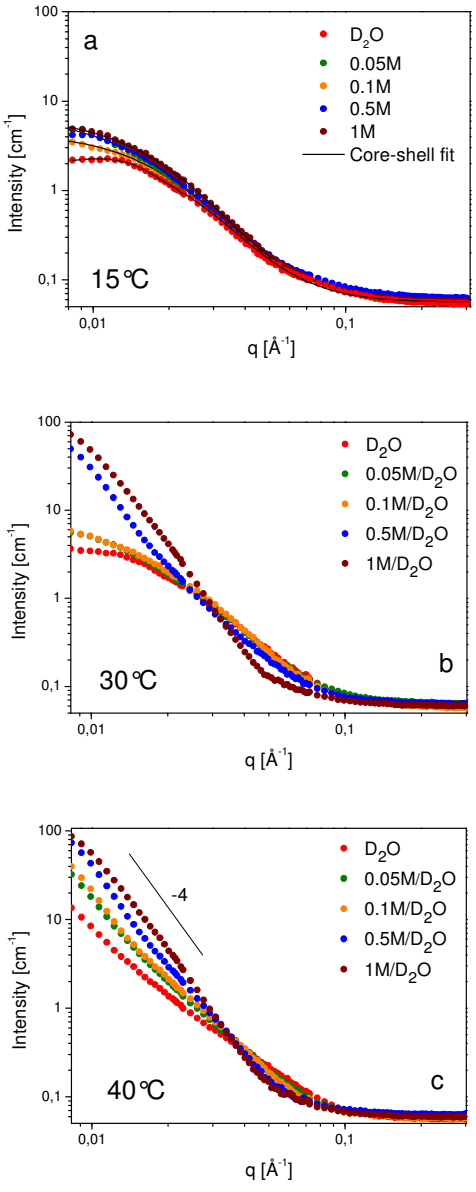

Fig 10 SANS patterns of 0.5wt% C_{18}-PEG_{10}-b-$PNIPAAM_{54}$-b-$PAMPS_{10}$ solutions at different levels of salt addition for the selected temperatures: a) 15 °C including core-shell model fits, b) 30 °C, c) 40 °C.

In Fig 10a is plotted the sample scattering at a temperature of 15°C, which is *below* the lowest CP for these samples (20 °C). As expected, we see that the scattering patterns are now quite similar for all samples, falling much closer than what was the case at 30 °C. The patterns are indicative of individual micelles, allowing for modelling of the SANS data. However, it should be noted that the samples may in addition contain some large intermicellar structures - as indicated by the DLS data presented earlier – that are outside the range accessible by SANS. The results of the core-shell modelling (cf. Eqs. 6-9), based on the patterns within the SANS region, are given in Table 1. The fitted curves at 15 °C are included in Fig 10a. For higher temperatures good fits could not be obtained, due to the formation of significantly larger structures.

Table 1. Structural parameters deduced from the model for C_{18}-PEG_{10}-*b*-$PNIPAAM_{54}$-*b*-$PAMPS_{10}$ in D_2O at different ionic strengths at 15 °C. R_c is the core radius, R_m the overall micellar radius, σ_m the smearing of the density profile, P the aggregation number, and B an instrumental background.

I/M	R_c/Å	R_m/Å	σ_m	P	B/cm^{-1}
0	14	32	1.34	21	0.057
0.05	17	54	0.99	40	0.058
0.1	15	84	0.45	26	0.050
0.5	16	91	0.42	34	0.060
1.0	17	60	0.77	39	0.052

We see that at 15 °C, well below CP, the polymer forms micelles with a relatively stable core size of about 2 x 15 Å, i.e., ca. 3 nm, and an overall diameter (2 R_m) of ca. 6 to 18 nm. Since the core at low temperature consists principally of C_{18}-blocks, one expects the core diameter to show little dependence on the ionic strength, as we also find in our data. The overall size can however be expected to vary significantly, since this will be strongly influenced by the interplay in the corona between hydrophilic and Columbic forces, and partial screening of the latter. The data in Table 1 indicate a gradual increase in the overall micelle size with increasing ionic strength (apart from at 1M salt), probably related to the screened electrostatic repulsions in the micellar corona. However, this does not translate into a clear trend in the aggregation number (P), which lies between 21 and 40 over the range of ionic strengths. Therefore, the effect of reduced

repulsion in the corona does not directly allow for more polymer chains to enter into the micelle, illustrating the complex interplay of forces involved. The characteristic micellar radius can be calculated from $R_{mic} = R_m(1+\sigma)$, which gives values from 75 Å at 0 M NaCl up to 129 Å at 0.5 M. Sigma generally decreases with increasing temperature signifying a more compact structure of the micelles. Thus the corona structure seems to undergo a transition from more diffuse to more compact larger micelles.

Finally, we may consider a temperature well *above* the CP for all samples. In Fig 10c, the sample scattering at a temperature of 40 °C is plotted, which is above the highest CP (35 °C). Contrary to what was observed at the lowest temperature (15 °C), we now see large differences in the patterns, and that the low-q intensity increases continuously with increasing distance between the actual temperature (40 °C) and the CP for each sample. This is most likely because the aggregation tendency (or stickiness) is drastically dependent on the distance above the CP for the sample in question. The slope is seen to approach a value of -4 at low q-values, indicating the formation of compact sphere-like entities.

Overall, the SANS data that probes structural changes on the nanoscale (here less than 100 nm) therefore compare well with the information from turbidity that is more sensitive to larger length scales. We see a conversion from micellar-like structures below CP to large intermicellar aggregates above CP for all samples. For this reason, at a certain temperature, e.g., 30 °C, we see considerable difference in particle size depending on the CP (and thus the ionic strength) of the considered sample. Furthermore, well below the CP for all samples, they show clear similarities with respect to particle size and shape, whereas above the CP they demonstrate large differences due to different degree of stickiness resulting in different aggregate sizes.

Conclusions

In this study we show how detailed information concerning the temperature dependence of the C_{18}-PEG_{10}-*b*-$PNIPAAM_{54}$-*b*-$PAMPS_{10}$ triblock copolymer can be gained by combining various techniques probing the range from nm to near µm scale. We show how the inclusion of charged PAMPS end-groups can strongly modify the temperature dependent hydrophobic restructuring when varying the level of salt addition. The transition point for creation of large micellar aggregates can be moved in steps from ca. 35 °C and as far down as 20 °C. We also show that an increase in temperature forces the charged segments out towards the micellar surface, because of the dehydration induced by the PNIPAAM blocks, an effect that can explain the strong influence of salt on the cloud point for this system. A simplified schematic illustration of the overall behavior of this system is given in Fig 11.

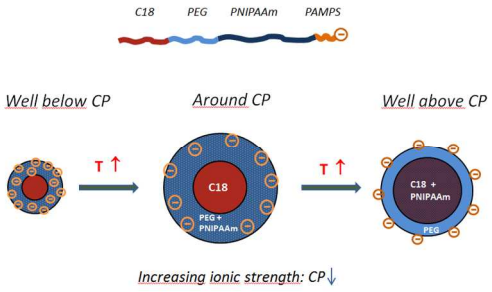

Fig 11 A simplified schematic illustration of the overall effect on the self-assembly of the amphiphilic copolymer at different conditions of temperature.

Initially, the polymer chains organize into small micellar structures, with a size of around 10 nm, as determined by SANS. The core consists mainly of the hydrophobic C_{18} end blocks, whereas the shell is a mixture of PEG and PNIPAAM, the latter being quite hydrophilic at low temperature. The charges are localized to the outer region of the shell. Upon heating, the stickiness of the PNIPAAM blocks increases and large association structures are formed around the cloud point with high charge density and the charges generally closer to the shell surface. Upon further heating, PNIPAAM is increasingly dehydrated and is probably forced towards the center of the association structures, sharing the core with the C_{18} chains. In this situation, the shell consists mainly of PEG chains, with a highly charged surface due to the PAMPS blocks. Overall, the present study exemplifies the large span in structural properties that can be achieved by combining blocks with hydrophobic, hydrophilic, and charged groups in the same polymer chain.

Acknowledgements

B.N. and R.L. greatly acknowledge a grant from the Norwegian Research Council, SYNKNØYT for the project with the number 8411/F50.

Notes and references

[a] *Department of Chemistry, University of Oslo, P.O. Box 1033, Blindern, N-0315 Oslo, Norway*
[b] *Department of Physics, Institute for Energy Technology, P. O. Box 40, N-2027 Kjeller, Norway*

** Corresponding authors: e-mail bo.nystrom@kjemi.uio.no, Phone: +47-22855522.*

1. P. Alexandridis, *Curr. Opin. Colloid Interface Sci.,* 1996, **1**, 490-501.
2. E. Cabane, X. Zhang, K. Langowska, C. Palivan and W. Meier, *Biointerphases,* 2012, **7**, 1-27.
3. I. W. Wyman and G. Liu, *Polymer,* 2013, **54**, 1950-1978.
4. L. F. Zhang and A. Eisenberg, *Polym. for Adv. Techn.,* 1998. **9**, 677-699.
5. J.-F. Gohy, *Block Copolymer Micelles*, In Block Copolymers II, V. Abetz, Editor, 2005, Springer, Berlin-Heidelberg, p. 65-136.
6. Roy, D., W.L.A. Brooks and B.S. Sumerlin, *Chem. Soc. Rev.,* 2013, **42,** 7214-7243.

7. C. Zhou, M.A. Hillmyer and T.P. Lodge, *Macromolecules* 2011, **44**, 1635-1641.
8. F. Ke, X. Mo, R. Yang, Y. Wang and D. Liang, *Macromolecules*, 2009, **42**, 5339-5344.
9. J. Chen, M. Liu, H. Gong, Y. Huang and C. Chen, *J. Phys. Chem. B*, 2011, **115**, 14947-14955.
10. O. V. Borisov and E.B. Zhulina, *Macromolecules,* 2002, **35**, 4472-4480.
11. S. Liu, J. V. M. Weaver, Y. Tang, N. C. Billingham and S. P. Armes, *Macromolecules,* 2002, **35**, 6121-6131.
12. Y. Bae, S. Fukushima, A. Harada and K. Kataoka, *Angew. Chem., Int. Ed.,* 2003, **42**, 4640-4643.
13. X.-L.Yang, Y.-L. Luo, F. Xu and Y.-S. Chen, *Pharm. Research,* 2014, **31**, 291-304.
14. R. Lund, L. Willner and D. Richter, *Adv. Polym. Sci.,* 2013, **259**, 51-158.
15. W. N. Yu, S. X. Liu, H. M. Wang and R. Tian, *J. Polym. Research,* 2012, **19**, 1-7.
16. S. Bayati, K. Zhu, L. T. T. Trinh, A.-L. Kjøniksen and B. Nyström *J. Phys. Chem. B*, 2012. **116**, 11386-11395.
17. S. Guragain, B. P. Bastakoti, S. I. Yusa and K. Nakashima, *Polymer,* 2010, **51**, 3181-3186.
18. S. Mishra, A. De and S. Mozumdar, *Synthesis of Thermoresponsive Polymers for Drug Delivery*, In Drug Delivery System, K.K. Jain, Editor. 2014, Springer, New York, p. 77-101.
19. H. Dautzenberg, Y. Gao and M. Hahn, *Langmuir,* 2000, **16**, 9070-9081.
20. Z. L. Quan, K. Z. Zhu, K. D. Knudsen, B. Nyström and R. Lund, *Soft Matter*, 2013, **9**, 10768-10778.
21. G. Masci, M. Diociaiuti and V. Crescenzi, *J. Polym. Sci., Part A: Polym. Chem.,* 2008. **46**, 4830-4842.
22. R. Pamies, K. Zhu, A. L. Kjøniksen and B. Nyström, *Polym. Bulletin* 2009, **62**, 487-502.
23. R. Pelton, *J. Colloid Interface Sci.,* 2010, **348**, 673-674.
24. R. Motokawa, S. Koizumi, M. Annaka, T. Nakahira and T. Hashimoto, *Prog. Colloid Polym. Sci.,* 2005, **130**, 85–96
25. X. Shi, J. Li, C. Sun and S. Wu, *Colloids Surf.,A,* 2000, **175**, 41-49.
26. J. Selb and Y. Gallot, *Makromol. Chem.,* 1981, **182**, 1775-1786.
27. C. M. Schilli, M. Zhang, E. Rizzardo, S. H. Thang, Y. K. Chong, K. Edwards, G. Karlsson and A. H. E. Műller, *Macromolecules*, 2004, **37**, 7861-7866.
28. Y. Xia, N.A.D. Burke and H.D.H. Stöver, *Macromolecules*, 2006. **39**, 2275-2283.
29. H. G. Schild and D.A. Tirrell, *J. Phys. Chem.*, 1990, **94**, 4352-4356.
30. Y. Mi Kyong, S. Yong Kiel, S. C. Chong and M. L. Young, *Polymer,* 1997, **38**, 2759-2765.
31. M. A. Behrens, M. Lopez, A. L. Kjøniksen, K. Zhu, B. Nyström and J. S. Pedersen, *Langmuir,* 2012, **28**, 1105-1114.
32. S. Zhou and B. Chu, *J. Phys. Chem. B,* 1998, **102**, 1364-1371.
33. A. L. Kjøniksen, M. T. Calejo, K. Zhu, A. M. S. Cardoso, M. C. P. De Lima, A. S. Jurado, B. Nyström and S. A. Sande, *J. Pharm. Sci.,* 2014, **103**, 227-234.
34. S. Qin, Y. Geng, D. E. Discher and S. Yang, *Adv. Mat.,* 2006, **18**, 2905-2909.
35. M. T.Calejo, S. A. Sande and B. Nyström, *Expert Opin. Drug Delivery,* 2013, **10**, 1669-1686.
36. B. Brugger and W. Richtering, *Adv. Mat.,* 2007, **19**, 2973-2978.
37. A. G. Rösler, W.M. Vandermeulen and H.-A. Klok, *Adv. Drug Delivery Rev.,*2012, **64,** 270-279.
38. M. Ciampolini and N. Nardi,.*Inorganic Chem.*, 1966, **5**, 1150-1154.
39. N. Beheshti, K. Zhu, A.-L. Kjøniksen, K. D. Knudsen and B. Nyström, *Soft Matter,* 2011, **7**, 1168-1175
40. W. Wang , H. Mauroy , K. Zhu , K. D. Knudsen, A.-L. Kjøniksen, B. Nyström and S. A. Sande,. *Soft Matter,* 2012, **8**, 11514-11525.
41. A. Dedinaite , E. Thormann, G. Olanya, P. M. Claesson, B. Nyström, A.-L. Kjøniksen and K. Zhu, *Soft Matter*, 2010, **6**, 2489-2498.
42. A.-L. Kjøniksen, K. Zhu, R. Pamies and B. Nyström, *J Phys. Chem. B,* 2008, **112**, 3294-9.
43. A.-L. Kjøniksen, K. Zhu, G. Karlsson and B. Nyström,. *Colloids Surf., A*, 2009, **333**, 32-45.
44. K. Zhu, J. Huiting, A.-L. Kjøniksen and B. Nyström, *J. Phys. Chem. B*, 2007, **111**,10862-10870.
45. J. D. Clogston and A.K. Patri, *Methods Mol. Biol.,* 2011, **697**, 63-70.
46. H. Jonassen, A.-L. Kjøniksen and M. Hiorth, *Colloid Polym. Sci.,* 2012, **290**, 919-929.
47. A. L. Kjøniksen, K. Zhu, M. A. Behrens, J. S. Pedersen and B. Nyström, *J. Phys. Chem. B,* 2011, **115**, 2125-2139.
48. A. L. Kjøniksen, A. Laukkanen, C. Galant, K. D. Knudsen, H. Tenhu and B. Nyström, *Macromolecules,* 2005, **38**, 948-960.
49. R. Kohlrausch, *Annalen der Physik* 1847, **148**, 353-405.
50. G. Williams and D.C. Watts, *Trans. Faraday Soc.,* 1970, **66**, 80-85.
51. M. A. Behrens, A. L. Kjøniksen, K. Zhu, B. Nyström and J. S. Pedersen, *Macromolecules,* 2012, **45**, 246-255.
52. C. Sommer, J. S. Pedersen and P. C. Stein, *J. Phys. Chem. B*, 2004, **108**, 6242-6249.
53. E. Halit, *Density measurement*, in *the measurement, instrumentation and sensors handbook on CD-ROM*. 1999, CRC Press.
54. J. S. Pedersen, C. Svaneborg, K. Almdal, I. W. Hamley and R. N. Young, *Macromolecules,* 2003, **36,** 416-433.
55. R. Lund, L. Willner, V. Pipich, I. Grillo, P. Lindner, J. Colmenero and D. Richter, *Macromolecules,* 2011, **44**, 6145-6154.
56. A. Malliaris, J. Le Moigne, J. Sturm and R. Zana, *J. Phys. Chem.,* 1985, **89**, 2709-2713.
57. M. Daoud and J. P. Cotton, *J. Phys.(France)* 1982, **43**, 531-538.
58. R. Lund, L. Wilner, J. Stelbrink, A. Radulescu and D. Richter, *Macromolecules,* 2004, **37**, 9984-9993.
59. Y.-L. Luo, L.-L. Zhang and F. Xu, *Chem. Eng. J.,* 2012, **189–190**, 431-442.
60. G. N. Malcolm and J. S. Rowlinson, *Trans. Faraday Soc.,* 1957, **53**, 921-931.
61. E. Karjalainen, N. Chenna, P. Laurinmäki, S. J. Butcher and H. Tenhu, *Polym. Chem.,* 2013, **4**, 1014-1024.
62. F. Hofmeister, *Arch. Exp. Pathol. Pharmakol* .,1888, **24**,247-260.
63. Y. Zhang and P. S. Cremer, *Curr. Opin. Chem.,* 2006, **10**, 658-663.
64. S. Fanaian, N. Al-Manasir, K. Zhu, A.-L. Kjøniksen and B. Nyström, *Colloid Polym. Sci.,*2012*,* **290**, 1609-1616.
65. S. Fujishige, K. Kubota and I. Ando, *J. Phys. Chem.,* 1989, **93**, 3311-3313.
66. H. G. Shild, *Prog. Polym. Sci*., 1992, **17**, 163-249.